Supplementary Materials

Surface-driven fast sodium storage enabled by Se-doped honeycomb-like macroporous carbon

Minglu Zhang[a], Meng Ning[a], Kairong Xiong[b,*], Zhihua Duan[a,c], Xiaoqing Yang[a], Zhenghui Li[a,*]

[a] School of Materials and Energy, Guangdong University of Technology, Guangzhou 510006, China

[b] School of Environmental Science and Engineering, Guangdong University of Technology, Guangzhou 510006, China

[c] Institute of Analysis, Guangdong Academy of Sciences, China National Analytical Center, Guangzhou 510006, China

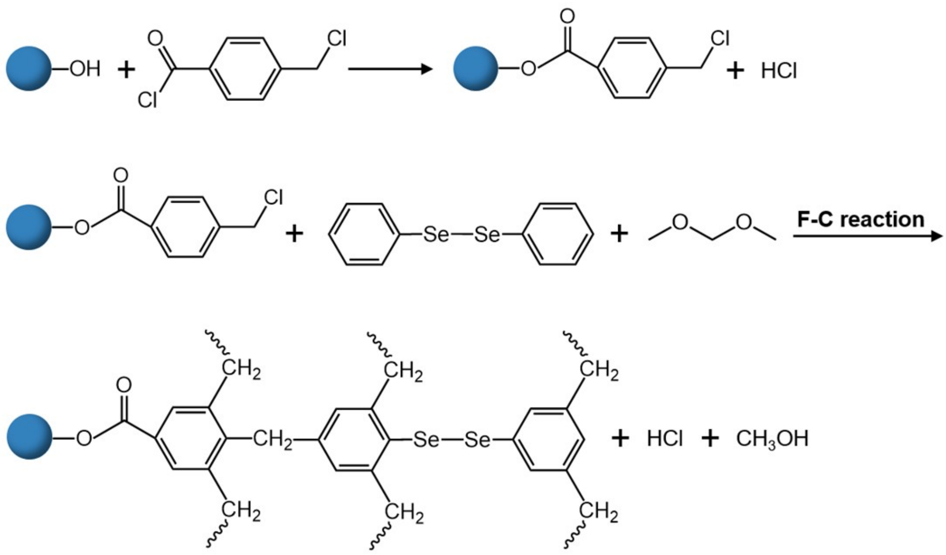

Fig. S1. The typical reaction mechanism of Se-HMC.

* E-mail addresses: xkr963@gdut.edu.cn (K. Xiong), lizhengh@gdut.edu.cn (Z. Li)

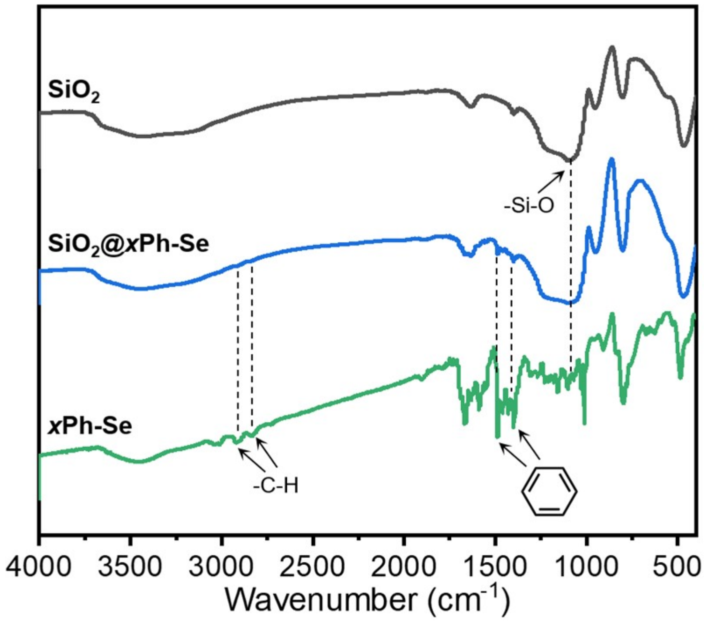

Fig. S2. FT-IR spectra of SiO_2, SiO_2@*x*Ph-Se, and *x*Ph-Se. The *x*Ph-Se is obtained by etching the SiO_2 template from SiO_2@*x*Ph-Se.

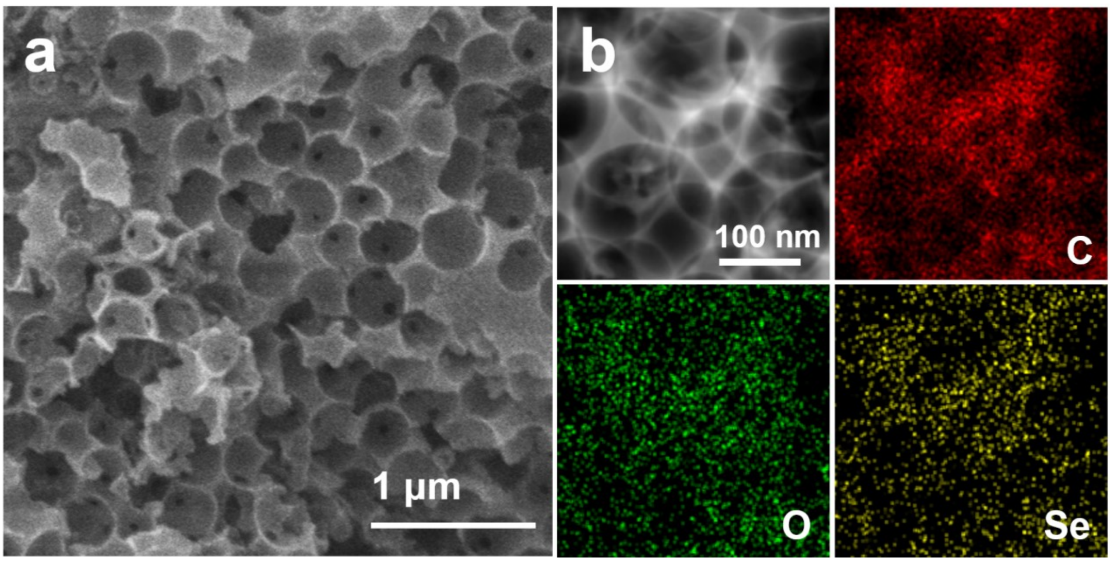

Fig. S3. Microstructural characterization of Se-HMC-500: (a) SEM image, (b) Dark-field TEM image, and corresponding elemental mapping images.

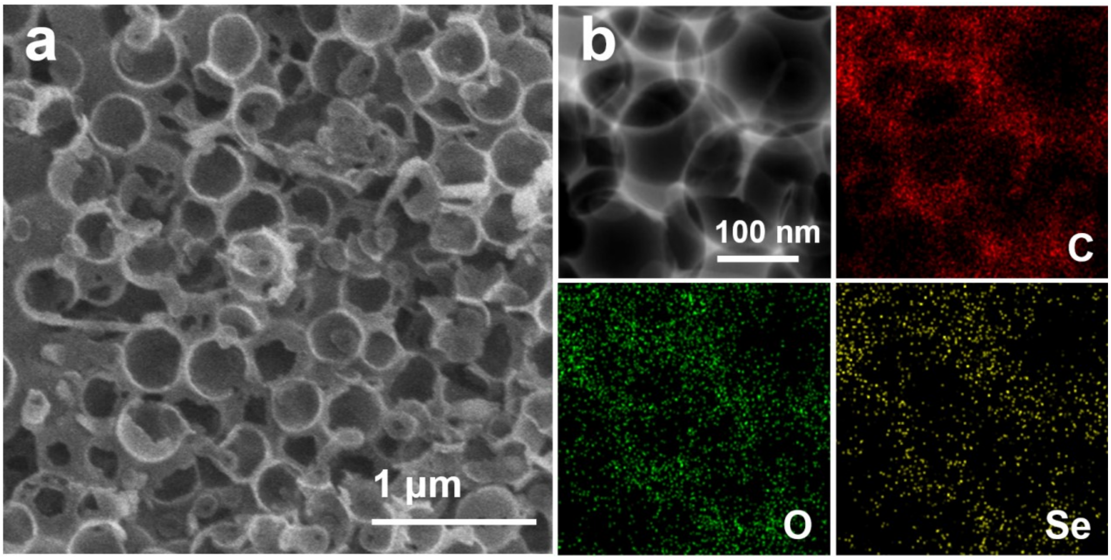

Fig. S4. Microstructural characterization of Se-HMC-700: (a) SEM image, (b) Dark-field TEM image, and corresponding elemental mapping images.

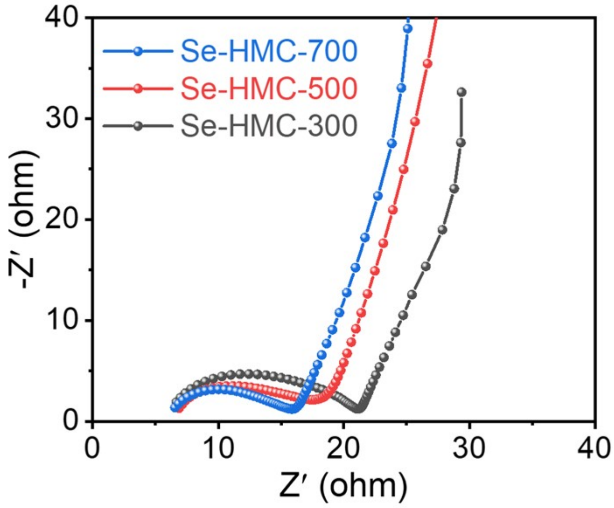

Fig. S5. The electrochemical impedance spectra of Se-HMC.

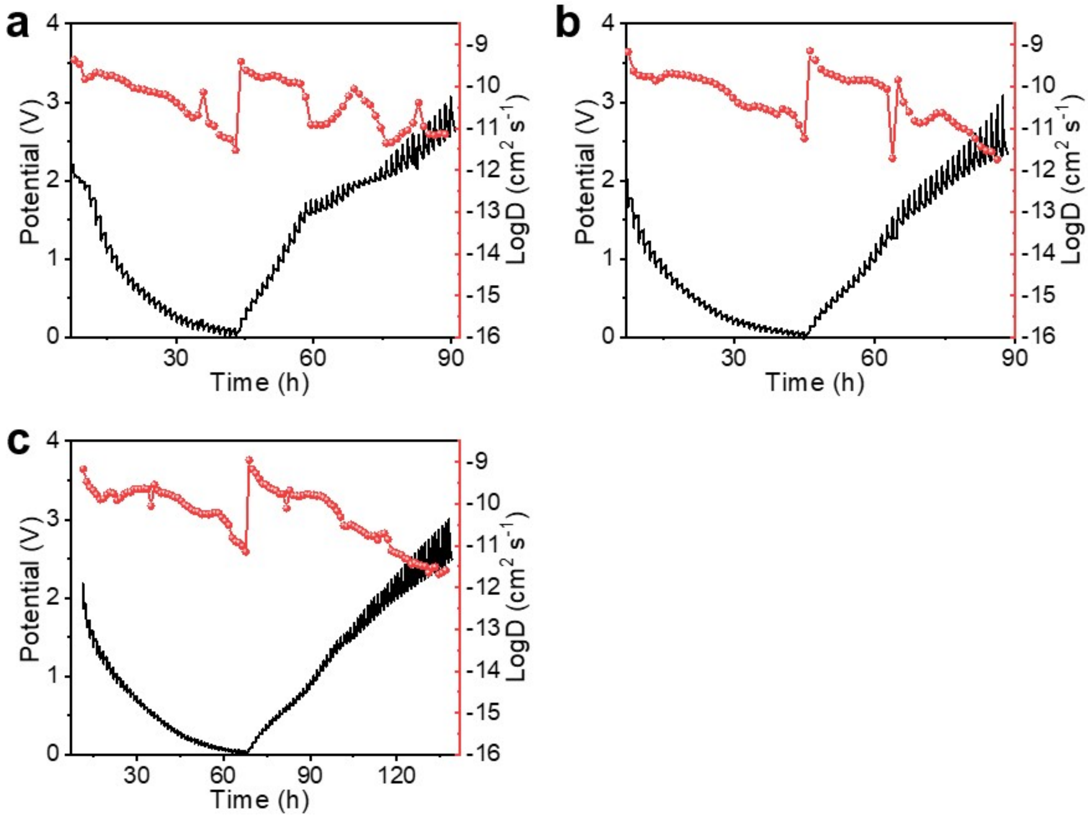

Fig. S6. The GITT curves of (a) Se-HMC-300, (b) Se-HMC-500 and (c) Se-HMC-700.

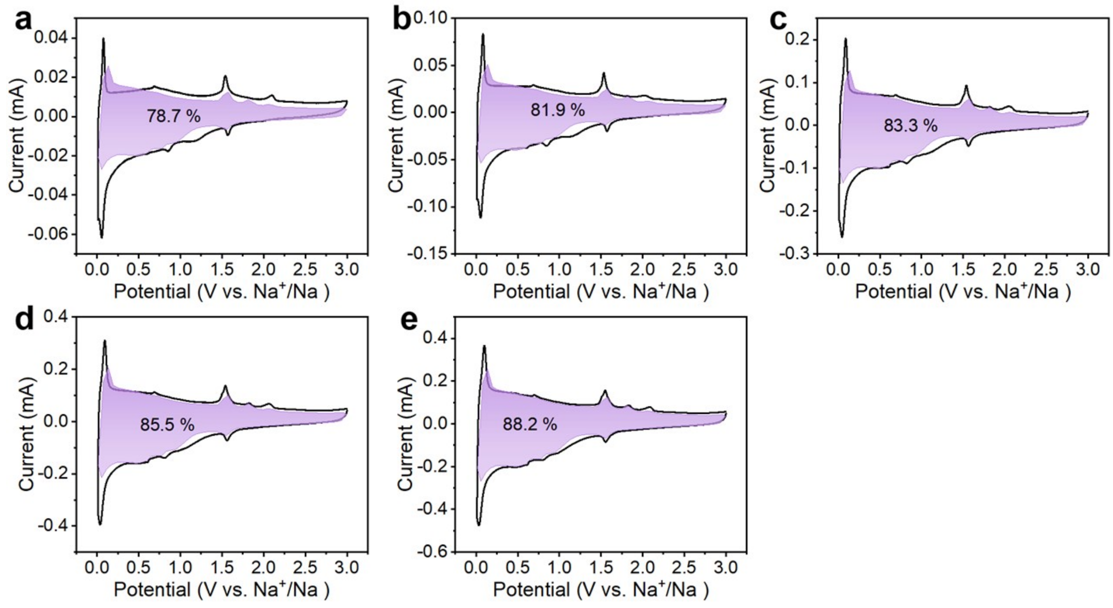

Fig. S7. CV curves displaying the capacitance contribution (purple area) to the total current at (a) 0.1, (b) 0.2, (c) 0.5, (d) 0.8, and (e)1 mV s^{-1} of Se-HMC-700.

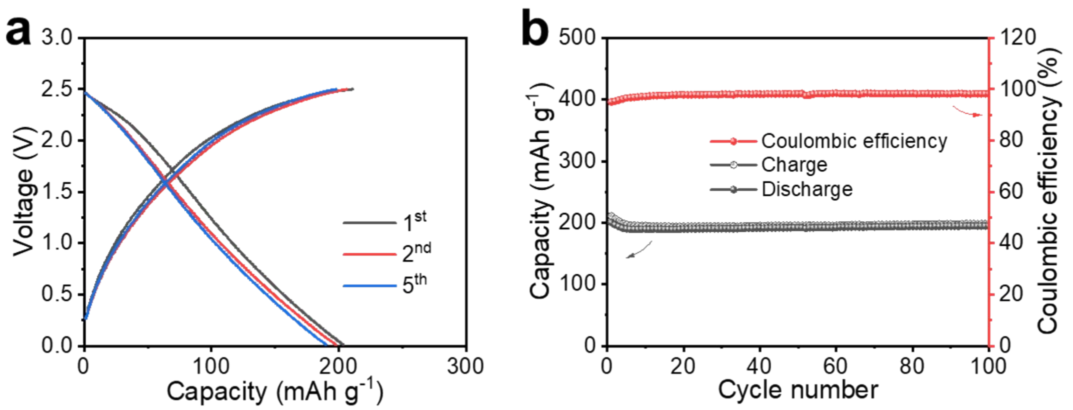

Fig. S8. The Na storage performance of $Na_3V_2(PO_4)_3$//Se-HMC-700 full cell: (a) galvanostatic charge/discharge curves for the 1st, 2nd and 5th cycles; (b) cycling stability with a current density of 0.1 A g^{-1}.

Table S1. The weight fractions of different elements calculated by XPS.

	C	Se	O
Se-HMC-300	56%	37%	7%
Se-HMC-500	80%	11%	9%
Se-HMC-700	77%	10%	13%

Table S2. Comparison of the rate capability for different types of carbon anodes.

Ref.	Sample	Capacity (low current density)		Capacity (high current density)		C_2/C_1
		I_1 (A g^{-1})	C_1 (mAh g^{-1})	I_2 (A g^{-1})	C_2 (mAh g^{-1})	
This work	**Se-HMC-700**	**0.1**	**334**	**5**	**251**	**75%**
[1]	Sugarcane waste-derived hard carbon	0.05	322.4	2	73.6	23%
[2]	N-doped carbon	0.05	343.2	2	129	38%
[3]	O-doped carbon	0.03	382	2	152	40%
[4]	B, N Co-doped carbon	0.05	296.1	5	101.3	34%
[5]	Pitch-based carbon	0.1	296	10	124	42%
[6]	N, S, P Co-doped carbon	0.1	281	5	100	36%

References

[1] K. Yu, X. Wang, H. Yang, Y. Bai, C. Wu, Insight to defects regulation on sugarcane waste-derived hard carbon anode for sodium-ion batteries, J. Energy Chem. 55 (2021) 499-508.

[2] S. Huang, D. Yang, X. Qiu, W. Zhang, Y. Qin, C. Wang, C. Yi, Boosting surface-dominated sodium storage of carbon anode enabled by coupling graphene nanodomains, nitrogen-doping, and nanoarchitecture engineering,

Adv. Funct. Mater. 32 (2022) 2203279.

[3] F. Sun, H. Wang, Z. Qu, K. Wang, L. Wang, J. Gao, J. Gao, S. Liu, Y. Lu, Carboxyl-dominant oxygen rich carbon for improved sodium ion storage: synergistic enhancement of adsorption and intercalation mechanisms, Adv. Energy Mater. 11 (2020) 2002981.

[4] Y. Tang, X. Wang, J. Chen, D. Wang, Z. Mao, Synthesis of presodiated B, N Co-doped carbon materials and application in sodium ions batteries with enhanced initial coulombic efficiency, Chem. Eng. J. 427 (2022) 131951.

[5] M. Hao, N. Xiao, Y. Wang, H. Li, Y. Zhou, C. Liu, J. Qiu, Pitch-derived N-doped porous carbon nanosheets with expanded interlayer distance as high-performance sodium-ion battery anodes, Fuel Process. Technol. 177 (2018) 328-335.

[6] D. Yang, S. Li, D. Cheng, L. Miao, W. Zhong, X. Yang, Z. Li, Nitrogen, sulfur, and phosphorus codoped hollow carbon microtubes derived from silver willow blossoms as a high-performance anode for sodium-ion batteries, Energ. Fuel. 35 (2021) 2795-2804.